IEEE Access
Multidisciplinary ⋮ Rapid Review ⋮ Open Access Journal

Received 14 September 2023, accepted 26 September 2023, date of publication 2 October 2023,
date of current version 10 October 2023.

Digital Object Identifier 10.1109/ACCESS.2023.3321304

RESEARCH ARTICLE

A Conical Cavity-Backed Antenna With Embedded Multiple Quarter-Wave Resonators

PHANUPHONG BOONTAMCHAUY[1], (Student Member, IEEE), RYUJI KUSE[2], (Member, IEEE), AND TAKESHI FUKUSAKO[2], (Senior Member, IEEE)
[1]Graduate School of Science and Technology, Kumamoto University, Kumamoto 860-8555, Japan
[2]Faculty of Advanced Science and Technology, Kumamoto University, Kumamoto 860-8555, Japan

Corresponding author: Ryuji Kuse (kuse@cs.kumamoto-u.ac.jp)

ABSTRACT A conical cavity-backed antenna with embedded multiple quarter-wave resonators (multiple QWRs) is proposed. The 3-dB axial ratio bandwidth (ARBW) of a cavity-backed antenna is limited by cavity resonance, undesired cavity current, and circular polarization (CP) behavior of the radiator. As a result, the cavity-backed antenna exhibits a high AR level and narrows the 3-dB ARBW, even though a high antenna gain and front-to-back ratio remain. In this study, a simple crossed-dipole was used to excite a conical cavity with four embedded multiple QWRs. The multiple QWR consists of two metallic plates and a cavity rim wall, which generate an additional current to support CP radiation. A conical cavity with embedded multiple QWRs can reduce the AR level and enlarge the 3-dB ARBW by preventing cavity resonance which creates a strong electric field inside the cavity, minimizing the effect of the undesired cavity current that radiates the cross-polarized wave, and further adding the CP mode to the antenna. The prototype realized a wide impedance bandwidth of 93.83% (1.72–4.76 GHz) and wide axial ratio bandwidth of 83.75% (1.86–4.54 GHz). The maximum gain was 9.9 dBic at 4.18 GHz. For the case where the radiator cannot be changed, this study demonstrates a cavity approach utilizing a microwave structure (multiple QWR) to reduce the AR level and maximize the 3-dB ARBW of a cavity-backed antenna without radiator modification.

INDEX TERMS Cavity-backed antenna, quarter-wave resonator, circular polarization, crossed-dipole.

I. INTRODUCTION

Many wireless communication applications use circularly polarized (CP) antennas for radio-frequency identification (RFID), mobile communication, satellite communication, and global navigation satellite systems (GNSS). Over the last decade, wireless communication systems have reached the limit of linearly polarized (LP) antennas for multiband and multifunctional applications. The major advantages of CP antennas over LP antennas are their reduced susceptibility to multipath interference, good polarization matching, and strong immunity to the Faraday effect.

A CP wave is composed of two orthogonal electric field components with an equivalent amplitude and a 90° phase difference [1]. A crossed-dipole antenna is widely used for CP radiation, which employs two half-wavelength dipoles that are placed orthogonally and fed by equal amplitudes in phase quadrature difference [2]. For simplicity, a vacant quarter phase-delay ring is used to create a single-feed crossed-dipole [3]. Because the crossed-dipole exhibits bidirectional radiation, a low directional gain is inevitable.

A CP antenna with a high gain, unidirectional radiation, and high front-to-back ratio is essential in modern wireless communication; thus, a perfect electrical conductor (PEC) is used as a reflector to back the crossed-dipole [4]. Moreover, an open metallic cavity is utilized, which resulted in a cavity-backed antenna with high gain and environmental isolation. To obtain a wide 3-dB axial ratio bandwidth (ARBW), the advanced radiators (crossed-dipole) and complicated feeding networks have been investigated.

Many modified crossed-dipoles have been published for wide 3-dB ARBW, such as crossed-dipoles with open stubs (49% ARBW) [5], asymmetric bowtie-shaped crossed-dipoles (51% ARBW) [6], triple-arm crossed-dipoles (51.4%

The associate editor coordinating the review of this manuscript and approving it for publication was Tutku Karacolak.

ARBW) [7], L-shaped crossed-dipoles (67.5% ARBW) [8], and elliptical crossed-dipoles (96.6% ARBW) [9]. A parasitic element has been introduced to generate additional resonances at the crossed-dipole. Several element shapes have been used, such as bowtie-shaped elements (58.6% ARBW) [10], triangular patches (63.4% ARBW) [11], truncated-corner patches (72.2% ARBW) [12], rectangular strips (90.9% ARBW) [13], square-slot patches (94.4% ARBW) [14], and sequentially rotated vertical metallic plates (106.1% ARBW) [15].

Other techniques have also been reported in the literature. A wideband feeding network acquired 48.6% ARBW [16]. Two baluns contributed 62.4% ARBW [17]. A crossed-dipole loaded with a magneto-electric (ME) dipole provided ARBW of 26.8% [18] and 45.3% [19]. The cross-slotted square patch for the magnetic current obtained 59.1% ARBW [20]. The rectangular dual cavity realized an ARBW of 66.7% [21]. The advanced crossed-dipole and composite cavity achieved a 120.1% ARBW [22].

However, this investigation focuses on cavity studies. Even though the cavity-backed structure provides a high gain and high front-to-back ratio, the 3-dB ARBW of the cavity-backed antenna is limited due to cavity resonance, undesired cavity current, and the radiator's CP behavior. These factors significantly increase AR levels. Therefore, for a situation where the radiator cannot be changed, a conical cavity-backed antenna with embedded multiple quarter-wave resonators (multiple QWRs) is proposed. A conical cavity with embedded multiple QWRs can enhance the antenna gain, prevent cavity resonance, minimize the effect of undesired cavity current, and add CP mode to the antenna, maximizing the 3-dB ARBW of the cavity-backed antenna. The prototype achieved a wide impedance bandwidth (IMBW) of 93.83% at $|S_{11}|$ of less than -10 dB and a wide 3-dB ARBW of 83.75%. The maximum gain was 9.9 dBic at 4.18 GHz.

II. ANTENNA STRUCTURE

The proposed antenna has a conical cavity with embedded multiple QWRs in the S-band. Fig. 1 shows the radiator (crossed-dipole) geometry of the antenna. It is constructed using two straightforward dipoles that are etched orthogonally on the top and bottom of 1.524 mm thick RO4003c material (48 mm $\times$ 48 mm, $\varepsilon_r = 3.38$, and $\tan\delta = 0.0027$). A vacant quarter ring connects the dipole arms such that a CP wave is produced because of a 90° phase delay between the two dipoles. The radiator is fed directly by a 50-ohm coaxial cable. A right-handed CP (RHCP) is generated in the $+z$ direction; otherwise, a left-handed CP (LHCP) is generated.

A conical cavity with four embedded multiple QWRs is shown in Fig. 2. A multiple QWR consists of two metallic plates and a cavity rim wall. The cavity is manufactured from aluminum. The cavity-backed antenna is assembled with the radiator positioned at the center and $\lambda_0/4$ distance above the bottom of the cavity (λ_0 is the wavelength at the CP minimum frequency of 2 GHz). All geometrical parameters are listed in Table 1. The overall dimensions of the proposed antenna are $1.06\lambda_c \times 1.06\lambda_c \times 0.38\lambda_c$ (λ_c is the wavelength at the CP center frequency of 3.2 GHz).

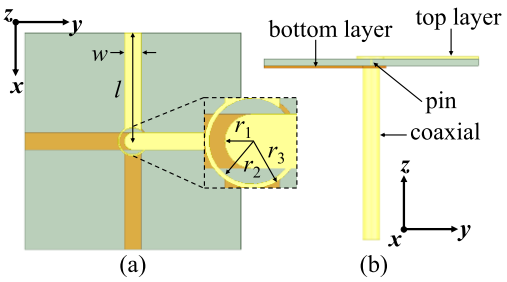

FIGURE 1. The radiator (crossed-dipole): (a) top view and (b) side view.

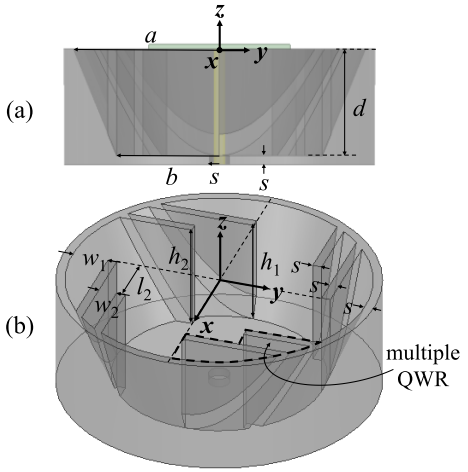

FIGURE 2. The proposed antenna: (a) side view and (b) 3D view (without the radiator).

TABLE 1. Geometrical parameters of the proposed antenna.

Parameter	Value [mm]	Parameter	Value [mm]
w	3.8	a	50
l	24	b	35
r_1	1.9	l_2	18
r_2	3	w_1	12
r_3	3.3	w_2	6
s	3	$d = h_1 = h_2$	36

Fig. 3 displays four different antenna models (Antenna I–IV) representing the antenna evolution. In particular, the models were developed without modifying the radiator; thus, the reflection coefficient remained unchanged across the S-band, as shown in Fig. 4. Fig. 5 shows a comparison of the simulated AR for each antenna model. Antenna I is a circular cavity-backed antenna (Fig. 3 (a)). The AR level of Antenna I increases to a high at 3.9 GHz due to cavity resonance. Antenna II is a conical cavity-backed antenna (Fig. 3 (b)). The conical shape shifts the effect of the cavity resonance to 4.7 GHz. Antenna III is a conical cavity-backed antenna with embedded QWRs (Fig. 3 (c)). The QWR is introduced to generate an additional current to resolve the high AR

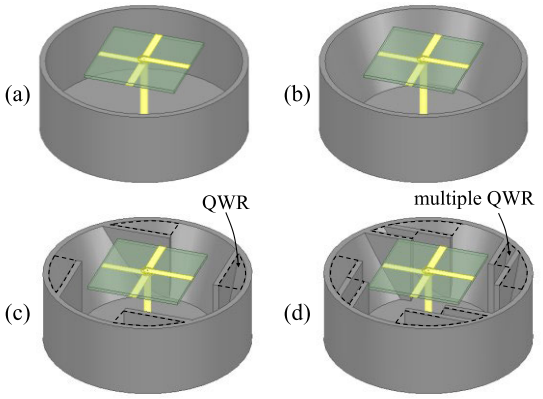

FIGURE 3. The antenna evolution: (a) Antenna I with circular cavity, (b) Antenna II with conical cavity, (c) Antenna III with conical cavity embedded QWRs, and (d) Antenna IV with conical cavity embedded multiple QWRs.

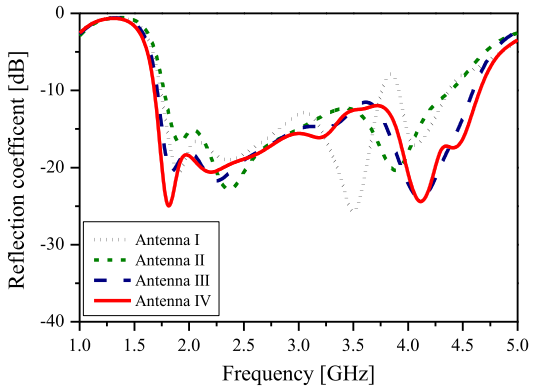

FIGURE 4. The simulated reflection coefficient for each antenna model.

(>3 dB) issue, caused by the undesired cavity current at higher frequencies. Antenna IV is the proposed antenna, which is a conical cavity-backed antenna with embedded multiple QWRs (Fig. 3 (d)). The multiple QWR can further enhance the 3-dB ARBW by adding a CP mode at 4.5 GHz to the antenna.

III. DESIGN AND MECHANISM

Although cavity-backed structures have advantages in terms of high gain, high front-to-back ratio, and environmental isolation, the 3-dB ARBW is limited due to cavity resonance, undesired cavity current, and radiator's CP behavior. These factors can cause high AR levels (>3 dB) in the boresight direction. Cavity resonance creates a strong electric field inside the cavity, resulting in a high AR level at the resonant frequency of the cavity resonator. At higher frequencies, the radiator induces an undesired cavity current with cross-polarized (XPOL) radiation, resulting in a high AR level. A high AR can also be a problem at higher frequencies because of the radiator's CP behavior; the CP radiator typically generates CP waves at lower frequencies but not at higher frequencies. For the case where the radiator cannot be changed, this section demonstrates a cavity design procedure

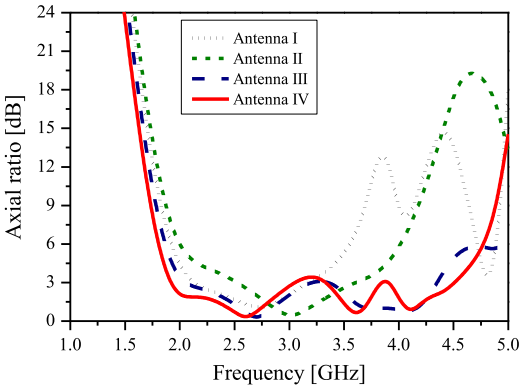

FIGURE 5. The simulated axial ratio for each antenna model.

that lowers the AR level and maximizes the 3-dB ARBW of a cavity-backed antenna without adjusting the radiator.

A. ANTENNA I

Antenna I is constructed using a crossed-dipole and an open circular metallic cavity. Although the circular cavity is a part of the antenna system, it can also be considered as a cavity resonator. The resonant frequency (f_r) of a circular cavity resonator can be determined by applying the following equations to the transverse magnetic (TM) and transverse electric (TE) modes [23]:

$$(f_r)^{TM}_{npq} = \frac{1}{2\pi a\sqrt{\varepsilon\mu}}\sqrt{x_{np}^2 + \left(\frac{q\pi a}{d}\right)^2} \quad (1)$$

$$(f_r)^{TE}_{npq} = \frac{1}{2\pi a\sqrt{\varepsilon\mu}}\sqrt{x_{np}'^2 + \left(\frac{q\pi a}{d}\right)^2} \quad (2)$$

where a is the cavity radius, d is the cavity height, x_{np} denotes the constant values for the TM mode, x'_{np} denotes the constant values for the TE mode [23], ε is permittivity, μ is permeability, $n = 0, 1, 2, \ldots, p = 1, 2, 3, \ldots$, and $q = 0, 1, 2, \ldots$ respectively.

Strong cavity resonance contributes to a strong electric field inside the cavity, resulting in a high AR level in the propagation direction. The resonant frequencies (f_r) of the TM_{010}, TM_{110}, and TE_{111} modes were calculated for different cavity radii (a), as shown in Fig. 6. The 50-mm radius is for the initial circular cavity because of the S-band in the range. Theoretically, the CP properties of Antenna I may be degraded by TM_{010} (2.2 GHz) and TM_{110} (3.6 GHz). Fig. 7 shows the electric field distribution of Antenna I which is obtained by using the HFSS electromagnetic field simulator. The results reveal that TM_{110} at 3.9 GHz generates a strong electric field. Therefore, the circular cavity must be modified into a conical cavity to minimize the effect of the strong electric field due to cavity resonance.

B. ANTENNA II

Antenna II is a conical cavity excited by a crossed-dipole. The conical structure is a combination of several circular radii. Therefore, the narrow part of the conical cavity can shift the

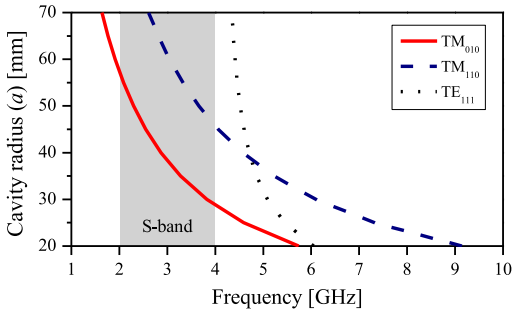

FIGURE 6. The calculated resonant frequency (f_r) of circular cavity resonator for different cavity radius (a).

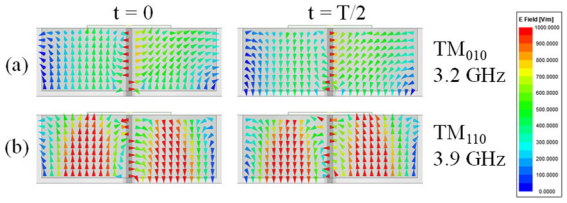

FIGURE 7. The electric field distribution of Antenna I (a = 50 mm) in xz plane: (a) TM_{010} at 3.2 GHz and (b) TM_{110} at 3.9 GHz.

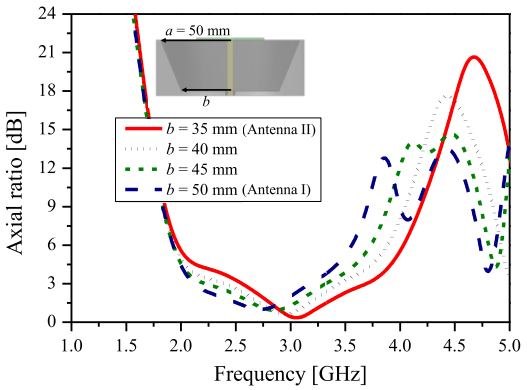

FIGURE 8. The simulated axial ratio of Antenna II for different conical radius (b).

effect of the cavity resonance to a higher frequency. Fig. 8 presents a comparison of the simulated AR for different conical radius (b). The shifting of the cavity resonant frequency (f_r) can be identified by the shifting of the peak AR point, as shown by b. The optimal value of b is 35 mm, at which point the cavity resonance left the operating band. Fig. 9 shows the electric field distribution of Antenna II at 3.2 and 3.9 GHz, verifying that the strong electric field due to cavity resonance was minimized.

To reduce the AR level and enhance the 3-dB ARBW of the cavity-backed antenna, the radiator and cavity currents of Antenna II were analyzed using the surface current density (J_{surf}). The position of J_{surf} along the propagation direction (z-axis) is very important in this step. Therefore, J_{surf} is simply classified into the aperture-J_{surf} ($z = 0$, at the radiator level) and reflector-J_{surf} ($z < 0$, below the radiator level).

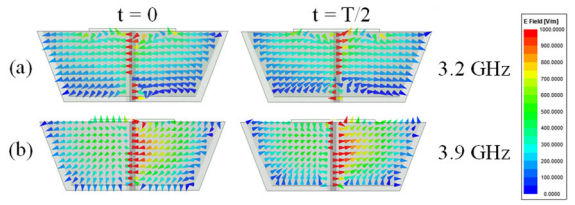

FIGURE 9. The electric field distribution of Antenna II (b = 35 mm) in xz plane: (a) 3.2 GHz and (b) 3.9 GHz.

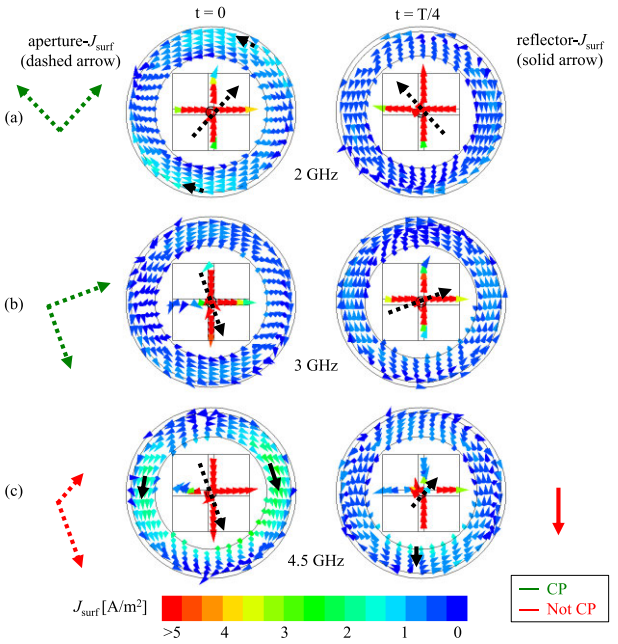

FIGURE 10. The current distribution of Antenna II: (a) 2 GHz, (b) 3 GHz, and (c) 4.5 GHz.

Fig. 10 illustrates the radiator and cavity currents of Antenna II. The cavity current can be represented by either the aperture-J_{surf} or reflector-J_{surf}, but the radiator current is only represented by the aperture-J_{surf}. In Fig. 10, the aperture-J_{surf} and reflector-J_{surf} are denoted by dashed and solid arrow styles respectively, in order to independently realize CP operation since their observation planes are different in the propagation direction (z-axis). The CP condition is obtained when the two vectors are equal in magnitude and have a 90° phase difference. Even both of aperture-J_{surf} and reflector-J_{surf} cannot be directly combined, but a synthesis is available in case that reflector-J_{surf} is sufficiently high. In Fig. 10 (c), the high AR issue at 4.5 GHz comes from two sources: the undesired cavity current produced by the radiator and the radiator's CP behavior. If the radiator cannot be changed and adjusted, the study proposes to solve the high AR issue due to the undesired cavity current by utilizing a cavity-embedded microwave structure. The radiator's CP behavior will then be addressed.

C. ANTENNA III

To minimize the effect of the undesired cavity current, a quarter-wave resonator (QWR) is proposed to be embedded inside the conical cavity. A transmission line can be used

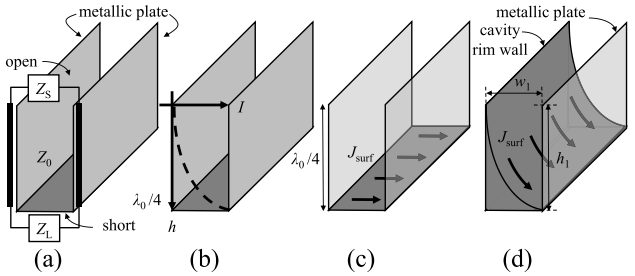

FIGURE 11. The quarter-wave resonator (QWR) at the resonant frequency: (a) transmission line model, (b) current intensity, (c) current distribution of symmetrical QWR, and (d) current distribution of asymmetrical QWR.

to describe the QWR as the simplest microwave resonator [24]. In a transmission line model, both the source and load impedances (Z_S and Z_L) can be considered, as shown in Fig. 11. At resonance, both Z_S and Z_L are reactive loads (capacitive or inductive). Therefore, no energy is delivered to the load, but the energy reflects and bounces between the two ends, indicating a standing wave. For the transverse resonance condition in a one-dimensional problem, the following equation can be used to determine the resonance condition:

$$1 = \Gamma_S \Gamma_L e^{-2j\beta_e h} \tag{3}$$

$$-1 = e^{-2j\beta_e h} \tag{4}$$

$$\beta_e h = p\pi/2, \quad p \text{ is odd} \tag{5}$$

where Γ_S and Γ_L are the reflection coefficients at the source and the load ends, respectively, β_e is some effective wavenumber for a z-propagating wave in a mixed medium, and h is the height or length of the transmission line.

In Fig. 11, a coupled vertical metallic plate with one closed end is considered as a microwave resonator using the transmission line principle. Due to the open and short-end configuration, the product of Γ_S and Γ_L is -1. This structure corresponds to a quarter-wavelength on the transmission line when p is set to 1 (the lowest mode). Any resonator with a height or length equal to a quarter-wavelength is a QWR. The electric current in an absolutely open circuit must be zero; however, it should not be zero when the structure is terminated by a short. Because the QWR generates additional current over the short end at the resonant frequency, the conical cavity with embedded QWR has the ability to minimize the effect of the undesired cavity current, resolving high AR issues.

According to Antenna II, the AR level tends to be low at 3 GHz (Fig. 8 (b = 35 mm)), where the radiator can perfectly generate CP waves, and the undesired cavity current is very small (Fig. 10 (b)), but high at 4.5 GHz. Although the additional current of the QWR may increase the AR level at 3 GHz (the fundamental frequency of the radiator), it can resolve the high AR issue at 4.5 GHz instead. Antenna III is a conical cavity-backed antenna with four embedded QWRs. The four QWRs are physically composed of four sequentially rotating metallic plates together with the cavity rim wall. Because the four QWRs are arranged in a sequential rotation, the direction of the additional current should be opposite to that of the undesired cavity current.

The relationship between the magnitude of the additional current and the undesired cavity current was examined to realize AR level reduction at 4.5 GHz. Fig. 12 shows the difference in the average magnitude of J_{surf} between zones I (avg$|J_{surf}|_{zoneI}$) and 0 (avg$|J_{surf}|_{zone0}$) in config. 1 (w_1 = 12 mm and l_1 = 12 mm), 2 (w_1 = 15 mm and l_1 = 6 mm), and 3 (w_1 = 12 mm and l_1 = 0 mm) at 3 and 4.5 GHz. The difference is written as:

$$\text{diff} = \text{avg}|J_{surf}|_{zoneI} - \text{avg}|J_{surf}|_{zone0} \tag{6}$$

Thus, the small difference (diff $\approx$ 0) implies that the additional and undesired currents cancel each other out in the radiation.

Fig. 13 shows the simulated AR in config. 1, 2, and 3. This study reveals that the AR level is reduced because of the QWR at 4.5 GHz. Furthermore, the small difference (diff $\approx$ 0) of config. 2 and 3 (Fig. 12 (b)) decreases AR level by 12 dB at 4.5 GHz. Since the config. 2 (Fig. 12 (a)) unintentionally obtains the excessive additional current (diff $\gg$ 0) at 3 GHz, the optimal configuration of the QWR is the config. 3 (w_1 = 12 mm and l_1 = 0 mm), where diff is sufficiently small for both 3 and 4.5 GHz. Antenna III enhanced the 3-dB ARBW from 32.26% (Antenna II) to 73.02% (2–4.3 GHz).

The AR reduction due to the QWR was analyzed using the radiated electric field pattern because the AR is calculated from the magnitude of the radiated electric field, as refers to (7). The radiated electric field was calculated using the equivalence principle [25]. The original fields that existed over a surface enclosing only the cavity section were used [26]. Fig. 14 compares the magnitudes of the radiated cross-polarized ($|E_{XPOL}|$) and co-polarized ($|E_{CoPOL}|$) electric field produced by the cavity at 4.5 GHz of Antenna II (without QWR) and Antenna III (with QWR). The cavity of Antenna III (with QWR) significantly reduces $|E_{XPOL}|$ and improves $|E_{CoPOL}|$ lowering the AR level at 4.5 GHz.

$$\text{AR} = (|E_{CoPOL}| + |E_{XPOL}|)/(|E_{CoPOL}| - |E_{XPOL}|) \tag{7}$$

Fig. 15 illustrates the current distribution of Antenna III with config. 3. In Fig. 15 (a) and (b), even the QWR generates additional current unintentionally at 2 and 3 GHz; however, this can be ignored because it has a small impact compared with the radiator current. As shown in Fig. 15 (c), an additional current at 4.5 GHz arises against the undesired cavity current.

The high AR problem at 4.5 GHz due to the undesired cavity current produced by the radiator was investigated. If the radiator cannot be modified, the QWR inside the cavity creates an additional current against the undesired cavity current, reducing the XPOL radiation of the cavity and decreasing the AR level at 4.5 GHz. At this frequency of Antenna III, the CP wave is only produced by the reflector-J_{surf} without a synthesis between aperture-J_{surf} and reflector-J_{surf}. The AR level at 4.5 GHz remains above the 3-dB level because of the radiator's CP behavior, which usually generates CP waves

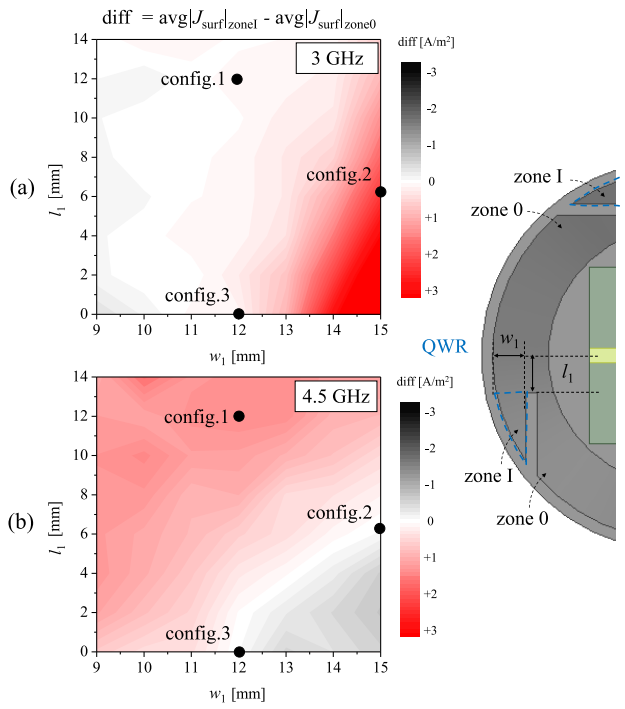

FIGURE 12. The difference in the average magnitude of surface current density between zone I and zone 0 of Antenna III for different w_1 and l_1: (a) 3 GHz and (b) 4.5 GHz.

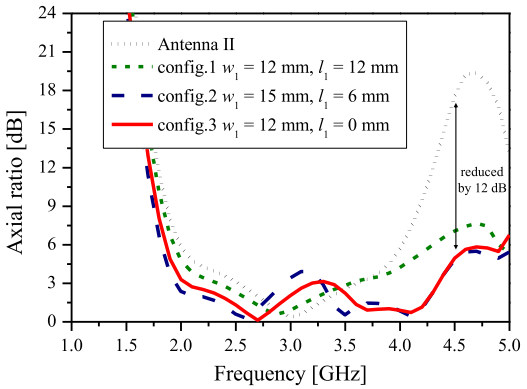

FIGURE 13. The simulated axial ratio of Antenna III for different w_1 and l_1 as config. 1, 2, and 3.

perfectly at lower frequencies but not at higher frequencies. To maximize the 3-dB ARBW without modifying the radiator, the conical cavity with embedded QWRs must be further modified utilizing a multiple QWR. This can add the CP mode to the antenna to resolve the high AR issue due to the radiator's CP behavior.

D. ANTENNA IV

In general, the CP mode can be easily added to the radiator by inserting a parasitic element, but this can result in impedance mismatching or frequency shifting; therefore, the antenna system must be further modified in relation to the change in the radiator. This study proposes a method for adding a CP

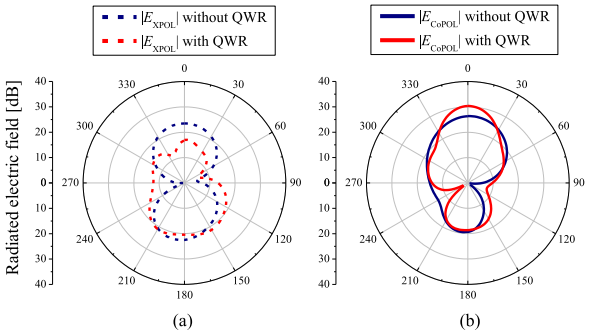

FIGURE 14. The simulated radiated electric field pattern produced by the cavity at 4.5 GHz of Antenna II (without QWR) and Antenna III (with QWR) in *xz* plane: (a) XPOL radiated electric field and (b) CoPOL radiated electric field.

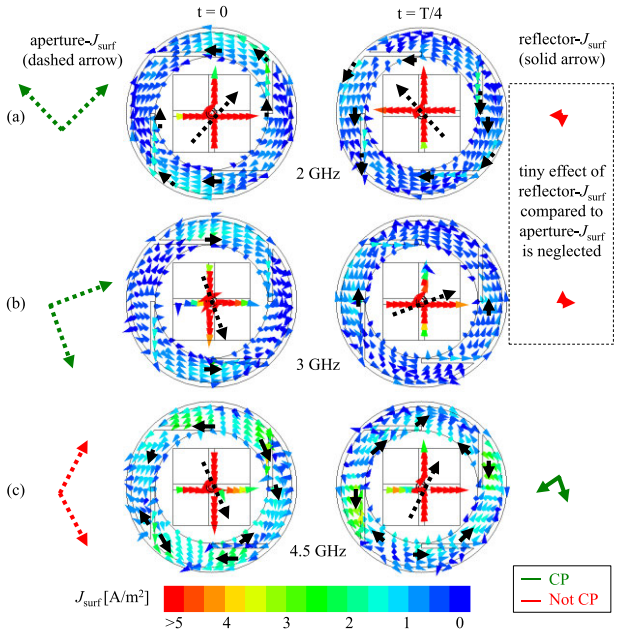

FIGURE 15. The current distribution of Antenna III with config. 3: (a) 2 GHz, (b) 3 GHz, and (c) 4.5 GHz.

mode utilizing the cavity approach. Antenna IV is fabricated by inserting four metallic plates into Antenna III, resulting in a conical cavity-backed antenna with four embedded multiple QWRs. The four multiple QWRs are a combination of eight metallic plates and a cavity rim wall. The multiple QWR can be divided into two parts: QWR_1 and QWR_2, as shown in Fig. 16. The objective of QWR_1 is similar to that of the QWR in Antenna III. The goal of QWR_2 is to add the CP mode at 4.5 GHz without disturbing the other frequencies (particularly the radiator's fundamental frequency of 3 GHz). For this purpose, QWR_2 must provide sufficient or moderate additional current at 4.5 GHz, but it must not provide additional current at 3 GHz. Fig. 16 shows the average magnitude of J_{surf} in zone II (avg$|J_{surf}|_{zoneII}$) of Antenna IV in config. A ($w_2 = 4$ mm and $l_2 = 20$ mm), B ($w_2 = 6$ mm and $l_2 = 18$ mm), C ($w_2 = 6$ mm and $l_2 = 12$ mm), D ($w_2 = 5$ mm and

TABLE 2. Performance comparison with reported circularly polarized cavity-backed antennas.

Ref.	Method	IMBW ($\|S_{11}\| \leq$ -10 dB) [%]	ARBW (AR $\leq$ 3 dB) [%]	Gain [dBic]	CP center frequency (f_c) [GHz]	Overall size [λ_c^3]
[5]	Radiator (rectangular-shaped adding open stub)	67.7	49	9.2	2.56	0.89×0.89×0.2
[6]	Radiator (asymmetric bowtie-shaped)	57	51	9.6	2.75	1×1×0.25
[7]	Radiator (triple-arm)	89.1	51.4	11.7	4.37	1.34×1.34×0.26
[8]	Radiator (L-shaped)	92.8	67.5	12.4	8	1.81×1.81×0.21
[9]	Radiator (elliptical shaped)	106.5	96.6	12	1.93	1.42×1.42×0.32
[10]	Element (bowtie-shaped patch)	68.9	58.6	9.4	2.9	0.79×0.79×0.27
[11]	Element (triangle-shaped patch)	78.3	63.4	4.5	1.42	0.46×0.46×0.1
[12]	Element (truncated-corner patch)	99.2	72.7	10	2.2	1.11×1.11×0.28
[13]	Element (rectangular strip)	93.1	90.9	8.6	4.3	1.07×1.07×0.4
[14]	Element (square-slot patch)	95.5	94.4	6.8	1.8	0.88×0.88×0.21
[15]	Element (vertical plate)	115.2	106.1	7	1.96	0.59×0.59×0.23
[16]	Feeding (wideband network)	54.7	48.6	3.5	1.43	0.33×0.33×0.17
[17]	Feeding (two baluns feeding)	70.6	62.4	4.8	2.79	0.65×0.65×0.35
[18]	ME dipole (loaded metallic horizontal plates and posts)	59.8	26.8	8	1.6	0.64×0.64×0.16
[19]	ME dipole (loaded metallic vertical and horizontal plates)	72.1	45.3	8.1	1.87	0.75×0.75×0.18
[20]	ME dipole (loaded crossed-slotted patch)	80	59.1	12.1	5.92	1.1×1.1×0.22
[21]	Cavity (dual square cavity)	79.4	66.7	9.7	3	0.86×0.86×0.36
[22]	Radiator (triangle and fan-shaped) and Cavity (composite)	125.2	120.1	12.2	4.4	1.85×1.85×0.41
This	Cavity (conical cavity with embedded multiple QWRs)	93.83	83.75	9.9	3.2	1.06×1.06×0.38

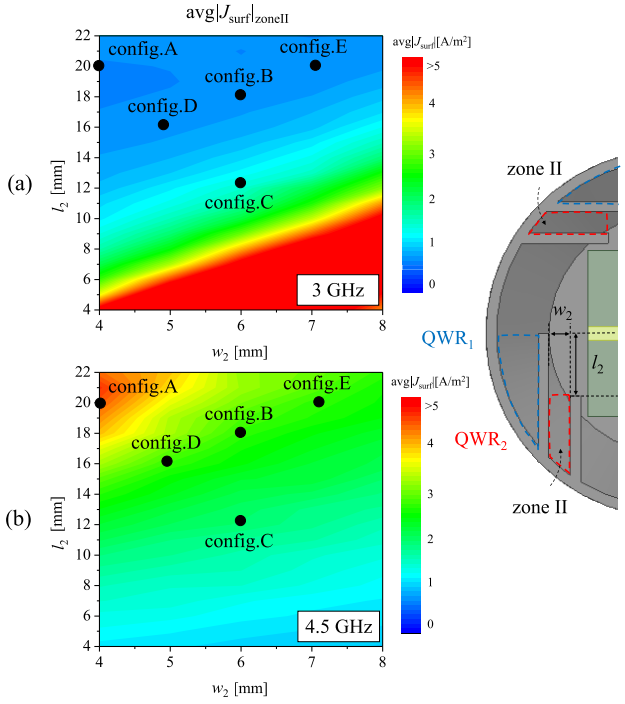

FIGURE 16. The average magnitude of surface current density inside zone II of Antenna IV for different w_2 and l_2: (a) 3 GHz and (b) 4.5 GHz.

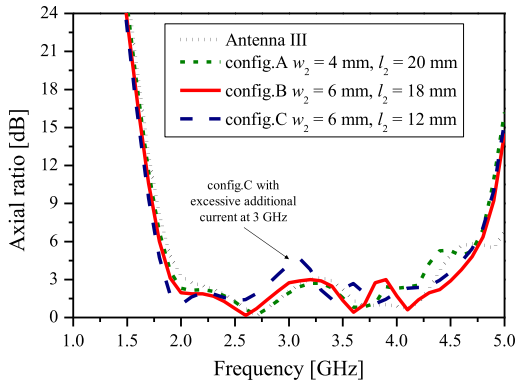

FIGURE 17. The simulated axial ratio of Antenna IV for different w_2 and l_2 as config. A, B, and C.

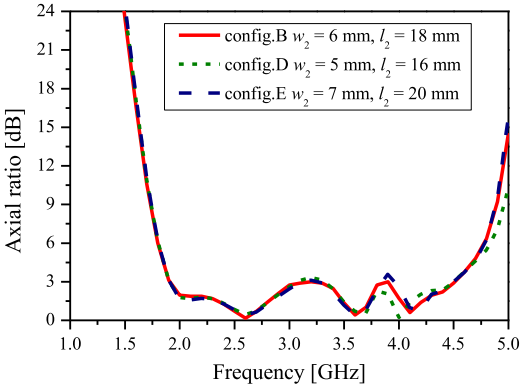

FIGURE 18. The simulated axial ratio of Antenna IV for different w_2 and l_2 as config. B, D, and E.

$l_2 = 16$ mm), and E ($w_2 = 7$ mm and $l_2 = 20$ mm) at 3 and 4.5 GHz.

Fig. 17 shows a comparison of the simulated AR in config. A, B, and C. Config. A can limit the additional current at 3 GHz, but it has excessive additional current at 4.5 GHz, preventing the addition of the CP mode at 4.5 GHz. Config. C unintentionally contributes to an additional current at 3 GHz, raising AR level at 3 GHz. There are several configurations that meet with the above requirement of a small additional current at 3 GHz and moderate at 4.5 GHz,

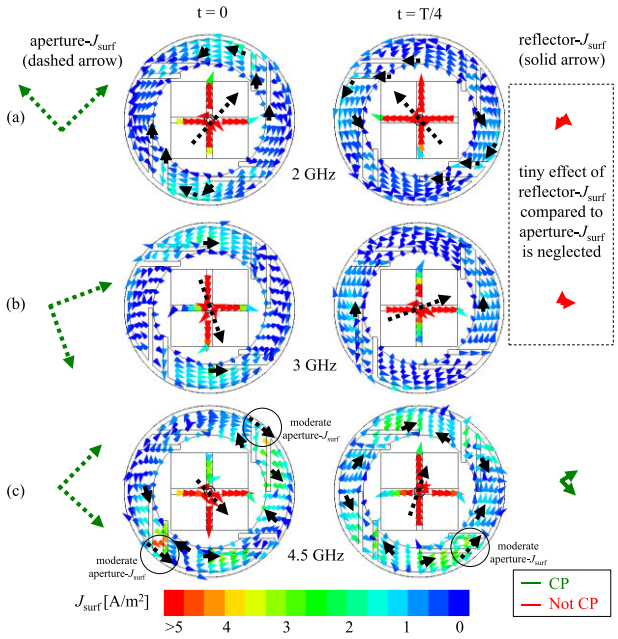

FIGURE 19. The current distribution of Antenna IV with config. B: (a) 2 GHz, (b) 3 GHz, and (c) 4.5 GHz.

FIGURE 20. The photographs of the proposed antenna.

for instance, config. B ($w_2 = 6$ mm and $l_2 = 18$ mm), D ($w_2 = 5$ mm and $l_2 = 16$ mm), and E ($w_2 = 7$ mm and $l_2 = 20$ mm). In Fig. 18, the simulated AR of config. B, D, and E show no significant differences in the CP properties. Therefore, config. B is the optimal configuration of the multiple QWR ($w_2 = 6$ mm and $l_2 = 18$ mm) for ease of fabrication. Consequently, a conical cavity with embedded multiple QWRs can add the CP mode to the antenna at a specific frequency without disturbing the other frequencies. Antenna IV decreased AR level to $\leq$3 dB at 4.5 GHz and achieved the wide 3-dB ARBW of 81.25% (1.9–4.5 GHz). Fig. 19 shows the current distribution in Antenna IV. Because QWR_2 generates an additional current close to the radiator level unlike QWR_1. In Fig. 19 (c), both aperture-J_{surf} and reflector-J_{surf} radiate CP wave in the high frequency range. The 3-dB ARBW of Antenna IV has been expanded by this band compared to that of Antenna III. Thus, the CP radiation in this expanded AR band of Antenna IV is a synthesis of two current distributions on the aperture-J_{surf} and reflector-J_{surf}.

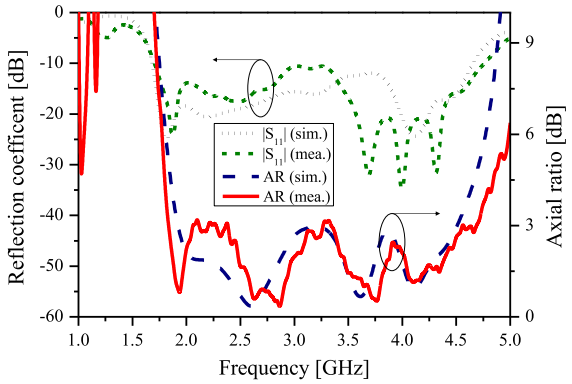

FIGURE 21. The simulated and measured reflection coefficient ($|S_{11}|$) and axial ratio of the proposed antenna.

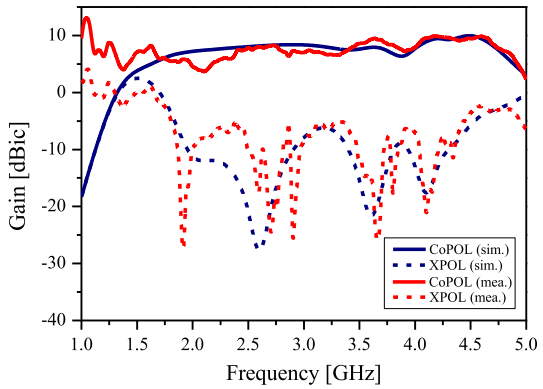

FIGURE 22. The simulated and measured gain of the proposed antenna.

IV. DESIGN GUIDELINES

Based on the study described above, the design guidelines for a conical cavity-backed antenna with embedded multiple QWRs are summarized as follows:

1) RADIATOR

We designed a bidirectional radiator that generated a CP wave in the desired operating band.

2) CIRCULAR CAVITY

The dimensions of the circular cavity were determined by avoiding cavity resonance and installing the radiator above the bottom of the circular cavity by $\lambda_0/4$.

3) CONICAL CAVITY

The circular cavity was modified into a conical shape by properly adjusting the conical radius (b) until the peak AR point left the band.

4) CONICAL CAVITY WITH EMBEDDED QWRS

Four metallic plates were sequentially rotated into the conical cavity, and a parametric study of w_1 and l_1 was conducted to determine the smallest difference between $\text{avg}|J_{surf}|_{zoneI}$ and $\text{avg}|J_{surf}|_{zone0}$ at frequencies where the undesired cavity current arises significantly.

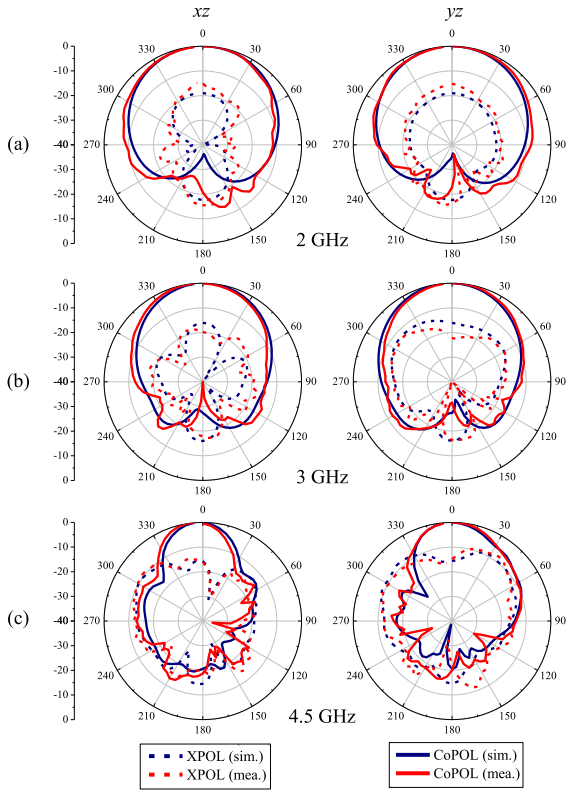

FIGURE 23. The simulated and measured normalized radiation pattern of the proposed antenna: (a) 2 GHz, (b) 3 GHz, and (c) 4.5 GHz.

5) CONICAL CAVITY WITH EMBEDDED MULTIPLE QWRS

Four metallic plates were inserted into the conical cavity embedded QWRs, and then a parametric study of w_2 and l_2 was performed to obtain moderate avg$|J_{\text{surf}}|_{\text{zoneII}}$ at a frequency that adds the CP mode (normally at the higher frequency) and the remaining low avg$|J_{\text{surf}}|_{\text{zoneII}}$ at other frequencies (especially the radiator fundamental frequency). Therefore, the aperture-J_{surf} which is created by QWR_2 could be an advantage.

V. EXPERIMENTS

A prototype of a conical cavity-backed antenna with embedded multiple QWRs (Antenna IV) was fabricated. Its photographs are shown in Fig. 20. Experiments were performed, and Fig. 21 presents the results of the reflection coefficient and AR. The simulated and measured IMBW ($|S_{11}| \leq -10$ dB) were 92.06% (1.7–4.6 GHz) and 93.83% (1.72–4.76 GHz), respectively, and the simulated and measured ARBW (AR $\leq$ 3 dB) were 81.25% (1.9–4.5 GHz) and 83.75% (1.86–4.54 GHz), respectively. The degradation of the measured reflection coefficient between 2.2 to 3.3 GHz could be attributed fabricating errors.

The antenna gain results are presented in Fig. 22. The simulated and measured gain showed maximum values of 10.14 dBic (4.5 GHz) and 9.9 dBic (4.18 GHz), respectively. The measured gain exhibited an error at a lower frequency because of the cutoff frequency of the reference antenna. Fig. 23 shows the normalized radiation patterns of the proposed antenna at 2, 3, and 4.5 GHz. To demonstrate the advantages of this study, Table 2 compares the performance of the proposed antenna and those in other studies. This study maximizes the 3-dB ARBW of a cavity-backed antenna using a pure-cavity approach without radiator adjustment. Other studies have attempted to increase the 3-dB ARBW using techniques that require highly accurate fabrication, such as advanced radiators and complicated feeding networks, which increase the complexity and difficulty of manufacturing.

VI. CONCLUSION

The 3-dB ARBW of a cavity-backed antenna is limited because of the high AR (>3 dB) issue due to cavity resonance, undesired cavity current, and radiator's CP behavior. At the resonant frequency of the cavity resonator, a strong electric field is created, resulting in a high AR level. The undesired cavity current also increases the AR level by producing an unwanted XPOL wave. In addition, high AR remains a problem because the CP behavior of the radiator is limited at higher frequencies. For the situation where the radiator cannot be changed, this study proposes a cavity approach to maximize the 3-dB ARBW. The study utilizes a conical cavity-backed antenna with embedded multiple QWRs. The conical shape of the cavity prevents cavity resonance in the operating band, thereby reducing the AR at the resonant frequency of the cavity resonator. Furthermore, the multiple QWR generates an additional current that cancels the undesired cavity current and adds the CP mode to the antenna, resulting in an AR level reduction at higher frequencies. The prototype achieved a wide IMBW ($|S_{11}| \leq -10$ dB) of 93.83% and wide 3-dB ARBW of 83.75%. The maximum gain was 9.9 dBic (4.18 GHz).

REFERENCES

[1] C. A. Balanis, *Antenna Theory: Analysis and Design*. Hoboken, NJ, USA: Wiley, 2015.

[2] S. X. Ta, I. Park, and R. W. Ziolkowski, "Crossed dipole antennas: A review," *IEEE Antennas Propag. Mag.*, vol. 57, no. 5, pp. 107–122, Oct. 2015, doi: 10.1109/MAP.2015.2470680.

[3] J. W. Baik, K. J. Lee, W. S. Yoon, T. H. Lee, and Y. S. Kim, "Circularly polarised printed crossed dipole antennas with broadband axial ratio," *Electron. Lett.*, vol. 44, no. 13, pp. 785–786, 2008, doi: 10.1049/el:20080794.

[4] Y. He, W. He, and H. Wong, "A wideband circularly polarized cross-dipole antenna," *IEEE Antennas Wireless Propag. Lett.*, vol. 13, pp. 67–70, 2014, doi: 10.1109/LAWP.2013.2296324.

[5] W. He, Y. He, and M. M. Tentzeris, "A novel wideband and circularly polarized cross-dipole antenna," *Wireless Commun. Mobile Comput.*, vol. 16, no. 17, pp. 3153–3162, Dec. 2016, doi: 10.1002/wcm.2743.

[6] H. H. Tran and I. Park, "Wideband circularly polarized cavity-backed asymmetric crossed bowtie dipole antenna," *IEEE Antennas Wireless Propag. Lett.*, vol. 15, pp. 358–361, 2016, doi: 10.1109/LAWP.2015.2445939.

[7] C.-E. Guan, T. Fujimoto, and S. Iwasaki, "3D-printed cavity backed crossed dipole antenna for high gain, wideband circular polarization in sub-6 GHz," *AEU-Int. J. Electron. Commun.*, vol. 158, Jan. 2023, Art. no. 154442, doi: 10.1016/j.aeue.2022.154442.

[8] X. Liang, J. Ren, L. Zhang, C. He, J. Geng, W. Zhu, and R. Jin, "Wideband circularly polarized antenna with dual-mode operation," *IEEE Antennas Wireless Propag. Lett.*, vol. 18, no. 4, pp. 767–770, Apr. 2019, doi: 10.1109/LAWP.2019.2902257.

[9] L. Zhang, S. Gao, Q. Luo, P. R. Young, Q. Li, Y.-L. Geng, and R. A. Abd-Alhameed, "Single-feed ultra-wideband circularly polarized antenna with enhanced front-to-back ratio," *IEEE Trans. Antennas Propag.*, vol. 64, no. 1, pp. 355–360, Jan. 2016, doi: 10.1109/TAP.2015.2501844.
[10] H. H. Tran, I. Park, and T. K. Nguyen, "Circularly polarized bandwidth-enhanced crossed dipole antenna with a simple single parasitic element," *IEEE Antennas Wireless Propag. Lett.*, vol. 16, pp. 1776–1779, 2017, doi: 10.1109/LAWP.2017.2676165.
[11] W. J. Yang, Y. M. Pan, and S. Y. Zheng, "A low-profile wideband circularly polarized crossed-dipole antenna with wide axial-ratio and gain beamwidths," *IEEE Trans. Antennas Propag.*, vol. 66, no. 7, pp. 3346–3353, Jul. 2018, doi: 10.1109/TAP.2018.2829810.
[12] Z. Zhao, Y. Li, M. Xue, L. Wang, Z. Tang, and Y. Yin, "Design of wideband circularly polarized crossed-dipole antenna using parasitic modified patches," *IEEE Access*, vol. 7, pp. 75227–75234, 2019, doi: 10.1109/ACCESS.2019.2920839.
[13] G. Feng, L. Chen, X. Wang, X. Xue, and X. Shi, "Broadband circularly polarized crossed bowtie dipole antenna loaded with parasitic elements," *IEEE Antennas Wireless Propag. Lett.*, vol. 17, no. 1, pp. 114–117, Jan. 2018, doi: 10.1109/LAWP.2017.2777442.
[14] L. Wang, W.-X. Fang, W.-H. Shao, B. Yao, Y. Huang, and Y.-F. En, "Broadband circularly polarized cross-dipole antenna with multiple modes," *IEEE Access*, vol. 8, pp. 66489–66494, 2020, doi: 10.1109/ACCESS.2020.2981050.
[15] Y. M. Pan, W. J. Yang, S. Y. Zheng, and P. F. Hu, "Design of wideband circularly polarized antenna using coupled rotated vertical metallic plates," *IEEE Trans. Antennas Propag.*, vol. 66, no. 1, pp. 42–49, Jan. 2018, doi: 10.1109/TAP.2017.2769690.
[16] C. Li, F.-S. Zhang, F. Zhang, and K. Yang, "A wideband circularly polarized antenna with wide beamwidth for GNSS applications," *Prog. Electromagn. Res. C*, vol. 84, pp. 189–200, 2018, doi: 10.2528/PIERC18041206.
[17] C.-Q. Feng, F.-S. Zhang, and F.-K. Sun, "A broadband crossed dipole antenna with wide axial ratio beamwidth for satellite communications," *Prog. Electromagn. Res. Lett.*, vol. 77, pp. 59–64, 2018, doi: 10.2528/PIERL18042606.
[18] S. X. Ta and I. Park, "Crossed dipole loaded with magneto-electric dipole for wideband and wide-beam circularly polarized radiation," *IEEE Antennas Wireless Propag. Lett.*, vol. 14, pp. 358–361, 2015, doi: 10.1109/LAWP.2014.2363944.
[19] H.-J. Zhang and F.-S. Zhang, "Circularly polarized crossed dipole with magnetoelectric dipole for wideband and broadbeam applications," in *Proc. Cross Strait Quad-Regional Radio Sci. Wireless Technol. Conf. (CSQRWC)*, Jul. 2018, pp. 1–3, doi: 10.1109/CSQRWC.2018.8455610.
[20] G. Feng, L. Chen, X. Xue, N. Li, and X. Shi, "Broadband CP crossed-stepped-dipole antenna incorporating a cross slotted square patch," *IET Microw., Antennas Propag.*, vol. 13, no. 3, pp. 340–345, Feb. 2019, doi: 10.1049/iet-map.2018.5254.
[21] T. K. Nguyen, H. H. Tran, and N. Nguyen-Trong, "A wideband dual-cavity-backed circularly polarized crossed dipole antenna," *IEEE Antennas Wireless Propag. Lett.*, vol. 16, pp. 3135–3138, 2017, doi: 10.1109/LAWP.2017.2764923.
[22] J. Fan, J. Lin, J. Cai, and F. Qin, "Ultra-wideband circularly polarized cavity-backed crossed-dipole antenna," *Sci. Rep.*, vol. 12, no. 1, pp. 1–10, Mar. 2022, doi: 10.1038/s41598-022-08640-z.
[23] R. F. Harrington, *Time-Harmonic Electromagnetic Fields*. New York, NY, USA: McGraw-Hill, 1961.
[24] S. Ramo, J. R. Whinnery, and T. Van Duzer, *Fields and Waves in Communication Electronics*. Hoboken, NJ, USA: Wiley, 1994.
[25] Y. Mushiake, "Self-complementary antennas," *IEEE Antennas Propag. Mag.*, vol. 34, no. 6, pp. 23–29, Dec. 1992, doi: 10.1109/74.180638.
[26] H. Nakano, K. Kikkawa, N. Kondo, Y. Iitsuka, and J. Yamauchi, "Low-profile equiangular spiral antenna backed by an EBG reflector," *IEEE Trans. Antennas Propag.*, vol. 57, no. 5, pp. 1309–1318, May 2009, doi: 10.1109/TAP.2009.2016697.

PHANUPHONG BOONTAMCHAUY (Student Member, IEEE) received the B.Sci. degree (Hons.) from the Civil Aviation Training Center (CATC), Suranaree University of Technology (SUT), in 2012, and the M.Eng. degree from the King Mongkut's University of Technology North Bangkok (KMUTNB), Bangkok, Thailand, in 2015. He is currently pursuing the Ph.D. degree with Kumamoto University, Kumamoto, Japan.

RYUJI KUSE (Member, IEEE) received the B.E., M.E., and Ph.D. degrees in engineering from Fukui University, Fukui, Japan, in 2011, 2013, and 2016, respectively. In 2017, he joined Kumamoto University, Kumamoto, Japan, as an Assistant Professor, where he is currently with the Department of Computer Science and Electrical Engineering. His research interests include meta-surface, MIMO antennas, and circularly polarized antennas and their applications. He is a member of IEICE.

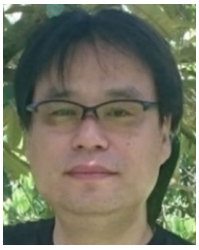

TAKESHI FUKUSAKO (Senior Member, IEEE) received the B.E., M.E., and Ph.D. degrees in engineering from the Kyoto Institute of Technology, Kyoto, Japan, in 1992, 1994, and 1997, respectively. In 1997, he joined Kumamoto University, Kumamoto, Japan, as a Research Associate, where he is currently a Professor with the Department of Computer Science and Electrical Engineering. From 2005 to 2006, he was a Visiting Researcher with the University of Manitoba, MN, Canada. He was a Visiting Associate Professor with the City University of Hong Kong, Hong Kong, SAR, China, from March 2015 to April 2015. His current research interests include antenna design, especially broadband antennas, circularly polarized antennas, and electrically small antennas and their applications. He is a Senior Member of IEICE. In 2014, he served as one of the TPC co-chairs for the 2014 IEEE International Workshop on Electromagnetics: Applications and Student Innovation Competition (iWEM2014). In 2017, he served as one of the general chairs for IEEE International Conference on Computational Electromagnetics (ICCEM2017). He served as an Associate Editor for the *IEICE Transactions on Communications*, from 2012 to 2016. He was also an Associate Editor of the IEEE TRANSACTIONS ON ANTENNAS PROPAGATION, from 2015 to 2022.